PRELIMINARY RESULTS ON NONCOLLOCATED TORQUE CONTROL OF SPACE ROBOT ACTUATORS

Scott W. Tilley, Colin M. Francis, Ken Emerick, and Michael G. Hollars

Ford Aerospace, Space Systems Division
Palo Alto, California 94303

Abstract

In the Space Station era, more operations will be performed robotically in space in the areas of servicing, assembly, and experiment tending among others. These robots may have various sets of requirements for accuracy, speed, and force generation, but there will be design constraints such as size, mass, and power dissipation limits. For actuation, a leading motor candidate is a DC brushless type, and there are numerous potential drive trains each with its own advantages and disadvantages. This experiment uses a harmonic drive and addresses some inhehrent limitations, namely its backdriveability and low frequency structural resonances. These effects are controlled and diminished by instrumenting the actuator system with a torque transducer on the output shaft. This noncolocated loop is closed to ensure that the commanded torque is accurately delivered to the manipulator link.

The actuator system is modelled and its essential parameters identified. The nonlinear model for simulations will include inertias, gearing, stiction, flexibility, and the effects of output load variations. A linear model is extracted and used for designing the noncolocated torque and position feedback loops. These loops are simulated with the structural frequency encountered in the testbed system. Simulation results are given for various commands in position. The use of torque feedback is demonstrated to yield superior performance in settling time and positioning accuracy.

An experimental setup being finished consists of a bench mounted motor and harmonic drive actuator system. A torque transducer and two position encoders, each with sufficient resolution and bandwidth, will provide sensory information. Parameters of the physical system are being identified and matched to analytical predictions. Initial feedback control laws will be incorporated in the bench test equipment and various experiments run to validate the designs. The status of these experiments is given.

1. Introduction

There are a wide variety of applications in space that could be assisted or performed telerobotically. These missions include large space structure assembly, module changeouts, maintenance, inspection, and refueling. This paper will assume a simple generic mission has been chosen to generate reasonable, preliminary manipulator requirements. A preliminary, symmetric arm configuration consists of two links with 7 degrees of freedom [1]. Obviously, arm mass and power requirements are to be minimized. Manipulator requirements are then reflected in the actuator subsystem sizing and component selection. This research focuses on the details of one

single degree of freedom joint at one end of the arm. Manipulator and derived joint requirements are given in Table 1.

Direct drive actuators initially appear attractive for space robotics because the manipulator is not required to support itself or a payload. However, there are needs of sustained tip forces to accelerate (or decelerate) payloads and to apply insertion forces during module changeouts. A 20 lb insertion force at the reach of 80 inches implies a 1600 in-lb (180 N-m) torque at the shoulder joint plus some margin. The size and mass of a direct drive joint would be large and yield a robot system design that was prohibitively expensive to launch and probably not capable of withstanding the thermal environment of space due to the high power dissipation.

Geared drives have the advantage of being lighter, requiring less power, and being more compact than an equivalent direct drive. However, gearing introduces a new set of problems to be overcome including, but not limited to: lower efficiency, various types of friction, torsional flexibility, backlash, reliability and life considerations. These issues can be adequately resolved and most space robot applications will employ some type of gearing.

Manipulator		Joint	
Manipulator Reach	2 m (79 in)	Gear Ratio	200
Maximum Tip Speed	0.5 m/sec	Maximum Joint Rate	0.25 rad/sec
Tip Position Resolution	0.001 m (0.04 in)	Joint Position Resolution	0.5 mrad
Sustained Tip Force	90 N (20 lbf)	Sustained Joint Torque	180 N-m
Tip Force Resolution	0.9N (0.2 lbf)	Joint Torque Resolution	1.8 N-m

Table 1: Manipulator and Joint Requirements

The gearing type chosen should ameliorate the worst effects for the given mission requirements at the expense of other effects to be compensated for. For instance, spur gears are efficient, but introduce backlash. The reduction of backlash, however, introduces compliance and so on. Applicable gearing systems such as spur gears, planetary gears, harmonic drives and others have been studied [2,3]. Of these, harmonic drives possess the best combination of performance characteristics for a space robot. They provide high gear ratios in one pass, have zero backlash, and have acceptable stiffness, friction, and efficiency. They are in current use in terrestrial robots and have been successfully used in spaceflight actuators.

Harmonic drives do present some problems that must be addressed before their use in a dexterous space manipulator. Motor friction is multiplied through the gearing producing undesirable tip force breakaway levels and a lack of adequate backdriveability. Imperfections in the gearing also produce output position errors at a frequency of twice the motor speed. This can cause vibration as the motor speeds up and down in a manuever and excites system resonances. The

harmonic drive dominates the manipulator compliance more than the links and this results in low system cantilever frequencies during large payload manipulations. The intelligent use of noncolocated torque feedback can drastically reduce these effects [4,5] by insuring that the joint actuator delivers commanded torque to the manipulator link. The servo control system must be designed to make the joint a linear device for applying torque. These loops will be first designed and simulated on a nonlinear joint model before being attempted in the digital control of the prototype joint.

2. Physical Actuator System

The testbed built includes the components required in a robot joint, but it is physically arranged to permit easy modification rather than represent an actual flight joint. The key elements of the testbed were chosen to meet the requirements set out previously in Table 1. The components and their nominal characteristics are presented in Table 2.

Motor	Type	DC, brushless
	Peak torque rating:	575 oz-in (4.06 N-m)
	Electrical time constant (τ_E)	4 msec
	Motor torque constant	60 oz-in./amp
	No load speed	1800 RPM
	Rotor inertia (J_{m1})	5.8 x10^{-4} kg-m^2
	Static friction	12 oz-in max
Input Bearings	Friction (B_{v1})	2 oz-in max
Harmonic Drive	Gear ratio (N)	200:1
	Maximum torque output	2890 in-lb (327 N-m)
	Torsional stiffness (K)	100,000 in-lb/rad initially, then stiffens
	Wave generator inertia (J_{m2})	1.8 x 10^{-4} kg-m^2
	Starting torque	11 oz-in
Torque Transducer	Rated capacity	5000 in-lb (565 N-m)
	Resolution	1:5000
	Torsional stiffness	750,000 in-lb/rad
Output Bearings	Friction (B_{v2})	40 oz-in max
Position Encoders	Resolution	1024 pulses per rev plus quadrature
	Frequency response	100 kHz

Table 2: Nominal Component Characteristics

The maximum speed and torque that the motor and harmonic drive will operate at during testing (still meeting slew requirements) is approximately one third of their rated capacity. The

various testbed transducers are adequate for meeting requirements. It is understood that a real system will have additional error sources such as misalignments, thermal distortions and others, but they are not addressed here. Highly precise end effector position and force measurements will ultimately require end point sensors and noncolocated end point control, whose benefits are being currently studied [6]. This does not detract from the significance of the noncolocated torque feedback loop. A brake is not currently used on the testbed joint because regenerative (dynamic) braking will be investigated in a parallel experiment.

3. Actuator System Model

A nonlinear model of the actuator plant containing the dominant physical phenomena is shown in Figure 1. The figure is a simple representation of the system and is not intended to reflect the physical layout of the joint. With the motor operated well below its no load speed, it will be capable of providing continuous demanded torque in the speed range used. The switching power amplifier used will not saturate under test conditions and it includes current feedback thus reducing back EMF effects.

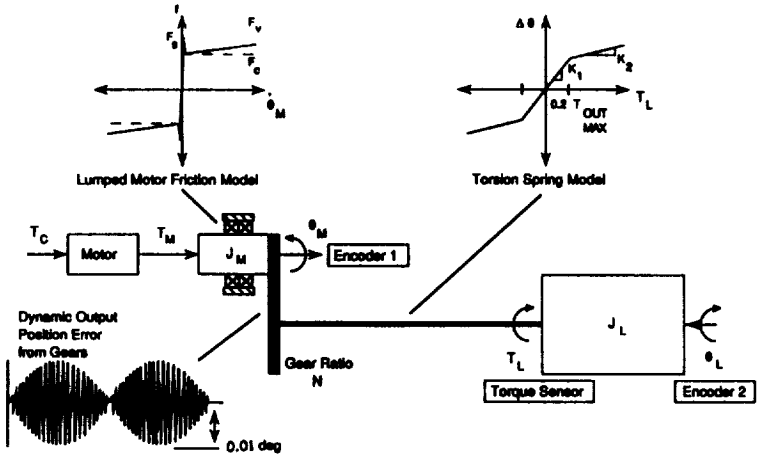

Figure 1: Nonlinear Model of Actuator

The dominant motor effect is inductance in the windings creating phase loss. The motor and wave generator inertias have been lumped together. Also, the friction model inboard of the harmonic drive gearing is lumped together into a static, Coulomb, and viscous friction model which will degradate output torque response when multiplied through the gearing. This friction model will be very difficult to verify experimentally and may change with component aging, therefore it is essential that the torque feedback loop be robust enough to handle a range of frictions. The position error at twice the motor speed due to gearing imperfections is modelled as a forcing disturbance torque. The compliance in the harmonic drive is modelled as a piecewise linear, stiffening spring. The mechanism stiffens as torque is applied because more surface area of the gear teeth are forced into contact. The cup, torque transducer, and load inertia are lumped together. Notice the output shaft rotation is opposite to the input shaft rotation. The sensor signals available are the motor

position θ_M (digital), output shaft position θ_L (digital) and torque T_L (analog). Additional phase loss will be introduced into the system through antialiasing filters and any differencing of position signals to get rate without tachometers. These key parameters are identified in vendor literature, but must be measured on the physical hardware in the testbed.

A simplified, linear model can be extracted by neglecting nonlinear friction and using one stiffness value and this will yield equations of motion (1), (2), and (3). Torque sensed at the load is due to spring and external (T_E) torques. From these, the colocated and two noncolocated transfer functions are derived and given in (4), (5), and (6). The numerical values in the transfer functions are based on the nominal testbed load inertia, J_L , of 3.0 kg-m^2 and a small amount of viscous bearing friction at the motor and output shaft (2 and 10 oz-in per rad/sec, respectively). The pole-zero patterns in the noncolocated transfer functions can easily destabilize a feedback system. Also note that output torque on the load cannot be maintained (zero DC gain) without an external torque. The system will simply spin up to a steady state speed (no load speed) where torque can no longer be generated at the output.

$$\tau_E \dot{T}_M + T_M = T_C \tag{1}$$

$$J_M \ddot{\theta}_M + B_{V1} \dot{\theta}_M + \frac{K}{N}\left(\frac{\theta_M}{N} - \theta_L\right) = T_M \tag{2}$$

$$J_L \ddot{\theta}_L + B_{V2} \dot{\theta}_L + K\left(-\frac{\theta_M}{N} + \theta_L\right) = T_E \tag{3}$$

and

$$\frac{\theta_M(s)}{T_C(s)} = \frac{(3.29 \times 10^5)(s^2 + 61.1^2)}{s(s + 16.9)(s + 250)(s^2 + 1.53s + 63.8^2)} \frac{\text{rad}}{\text{N-m}} \tag{4}$$

$$\frac{\theta_L(s)}{T_C(s)} = \frac{(6.14 \times 10^6)}{s(s + 16.9)(s + 250)(s^2 + 1.53s + 63.8^2)} \frac{\text{rad}}{\text{N-m}} \tag{5}$$

$$\frac{T_L(s)}{T_C(s)} = \frac{(1.84 \times 10^7)s}{(s + 16.9)(s + 250)(s^2 + 1.53s + 63.8^2)} \frac{\text{N-m}}{\text{N-m}} \tag{6}$$

This analysis can be modified and applied to the case where the load inertia is constrained from moving and torque is simply transmitted to the environment. This simulates a manipulator in contact with a fixed object and assumes a rigid link (arm). By setting the load angle and its derivatives to zero (or making the load inertia extremely large) in equations (1) through (3), the joint equations of motion for applying force to a fixed surface become evident. The resulting transfer functions are equations (7) and (8).

$$\frac{\theta_M(s)}{T_C(s)} = \frac{(3.29 \times 10^5)}{(s + 250)(s^2 + 18.4s + 19.2^2)} \frac{\text{rad}}{\text{N-m}} \quad (7)$$

$$\frac{T_L(s)}{T_C(s)} = 56 \frac{\theta_M(s)}{T_C(s)} \frac{\text{N-m}}{\text{N-m}} \quad (8)$$

A physical manipulator will attach to and move payloads. This creates large changes in the apparent inertia of the arm. It is instructive to look at the magnitude of the cantilever and free-free resonances and their relative separation as loads vary. The load inertia is matched to the motor and gearing through the square of the gear ratio. Table 3 below shows a range of frequencies with various load inertias. Asymptotically as the outboard load increases, the free-free frequency will approach the cantilever frequency in the matched case. This is a case of the tail wagging the dog as the motor cantilevers while the load remains stationary. Colocated proportional-derivative controller historically used in servo controls usually perform no better in bandwidth than about half the cantilever frequency [6].

Outboard Inertia (kg-m^2) and [matched inertia ratio $J_L/J_M N^2$]	Frequencies (rad/sec)	Comment
3 [0.1]	$\omega_c = 61.1, \zeta=0.00$ $\omega_f = 63.8, \zeta=0.01$	Testbed range
30 [1.0]	$\omega_c = 19.3, \zeta=0.00$ $\omega_f = 25.7, \zeta=0.16$	Matched case $\omega_f = \omega_c \sqrt{2}$
60 [2.0]	$\omega_c = 13.7, \zeta=0.00$ $\omega_f = 21.8, \zeta=0.26$	Unloaded manipulator arm
600 [20.0]	$\omega_c = 4.30, \zeta=0.00$ $\omega_f = 19.3, \zeta=0.45$	Manipulator with payload

Table 3: Structural Frequency Variations with Load Inertia Variations

4. Control Design and Simulation

Control analysis is performed to yield a suitable feedback controller to meet the requirements of Table 1, especially in position and force resolution at the tip. Simple root locus and Linear Quadratic Gaussian (LQG) techniques are used to derive compensator transfer functions for both position and torque feedback [7]. Output feedback will be used, not full state feedback [8]. The closed loop results for small slews in position are then evaluated for further refinement of the control algorithm. All controllers designed will operate within the actuator torque and bandwidth capabilities.

First, a colocated position feedback loop is derived. The open loop transfer function, equation (4), is dominated by the rigid body poles. A simple lead filter is chosen. The resonant mode is effectively

trapped by the cantilever zero. Physically, the mode is difficult to observe through the motor angle and difficult to actively damp. An angle slew at 0.25 rad/sec representing 20 cm of tip motion is performed using the full nonlinear simulation, see Figure 2. Load angle (synonymous for joint angle) is commanded by simply commanding a motor angle multiplied by the gearing. Notice the undesirable ringing in the load after the motor shaft has locked up under stiction. The load motion no longer has access to the energy dissipation mechanisms in the motor and relies on outboard structural and bearing damping alone. Joint position settles slowly and meeting requirements may not be possible without accurate knowledge of the stiction levels. Torque commands are also difficult to achieve across the joint due to stiction and the nonlinear spring. Notably, a minimum tip force of 17.5 N (3.9 lbf) is needed to break motor stiction.

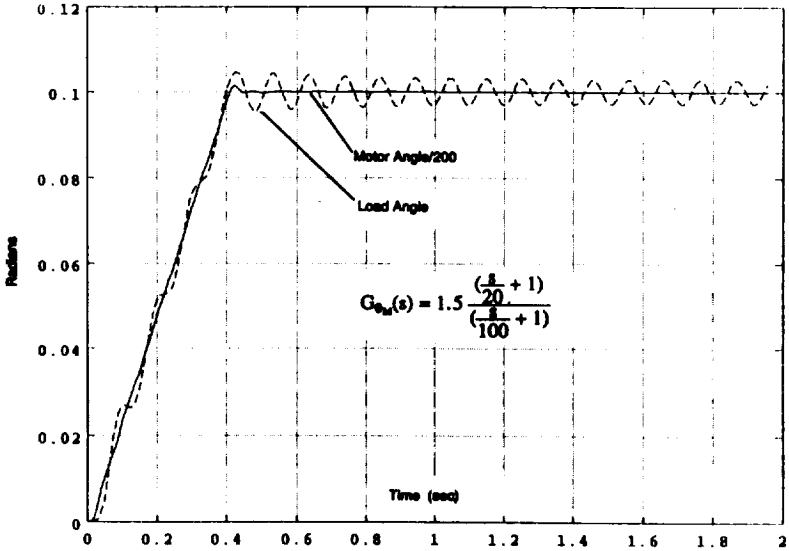

Figure 2: Position Slew With Colocated Angle Feedback

Second, a noncolocated position feedback loop is derived. The open loop transfer function, equation (5), is first approximated by the rigid body poles and the resonance while ignoring the motor inductance. A reduced order compensator is designed using LQG regulator techniques with output weighting. A root locus of this compensation with the linear plant model is given in Figure 3. In the absence of the cantilever zeroes, the resonances can be actively damped at the expense of increased motor activity. This compensation was applied to the nonlinear simulation.

This closed loop system is slewed using the full nonlinear plant model simulation, see Figure 4. The load angle no longer rings although the rigid body performance is slightly slower. The steady state error due to motor stiction for this compensator is still above the position requirement. Increased compensator gain is necessary, but limit cycling quickly occurred with higher gains. Also, there exists the potential for control spillover with higher gain. Finally, this loop cannot be used for controlling output torque levels when the joint is in contact with the environment as the load angle is fixed.

Thus far, the position controllers have failed to provide adequate servo performance regardless of the feedback sensor location. Perfect knowledge of the plant dynamics and parameters can yield

feedforward compensation, but feedback techniques are preferred for robustness. Output torque feedback is the solution. This may be achieved through successive loop closure techniques or full multi-input multi-output (MIMO) LQG design. Both are tried here.

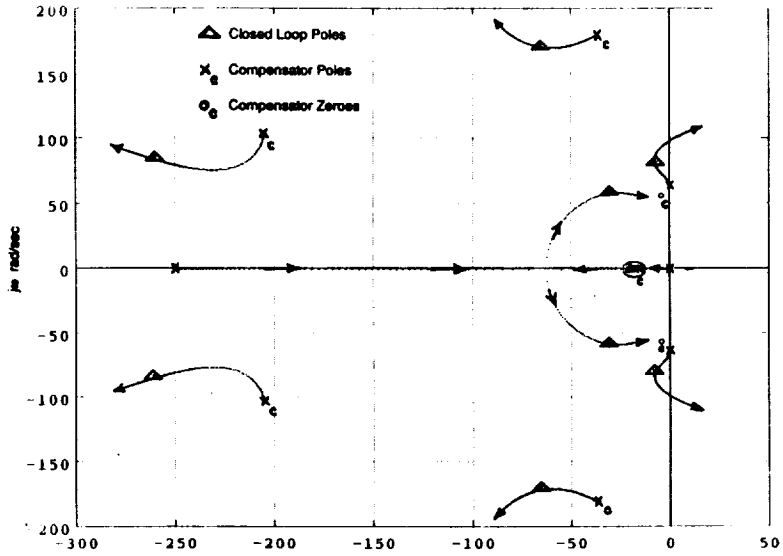

Figure 3: Noncolocated Position Feedback Root Locus

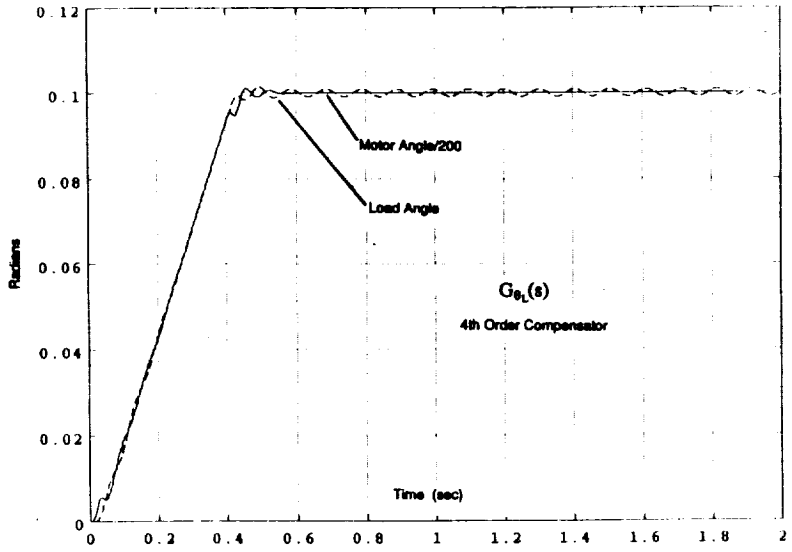

Figure 4: Position Slew With Noncolocated Position Controller

First, a simple lead filter stabilizes the noncolocated torque loop and both actively damps the load resonance and reduces the friction effects observed on the load side of the gearing. Next, the simple colocated position loop is closed around the torque inner loop. This produced good position performance during the slew shown in Figure 5. This design also yielded good torque response with the joint in contact for torques that did not exceed the first linear region of the spring. Higher torque commands resulted in instabilities due to the higher effective loop gain. Finally, both noncolocated

loops (position and torque) are closed simultaneously using LQG techniques. This controller regulates load angle well and effectively damps vibration during the slew in Figure 6.

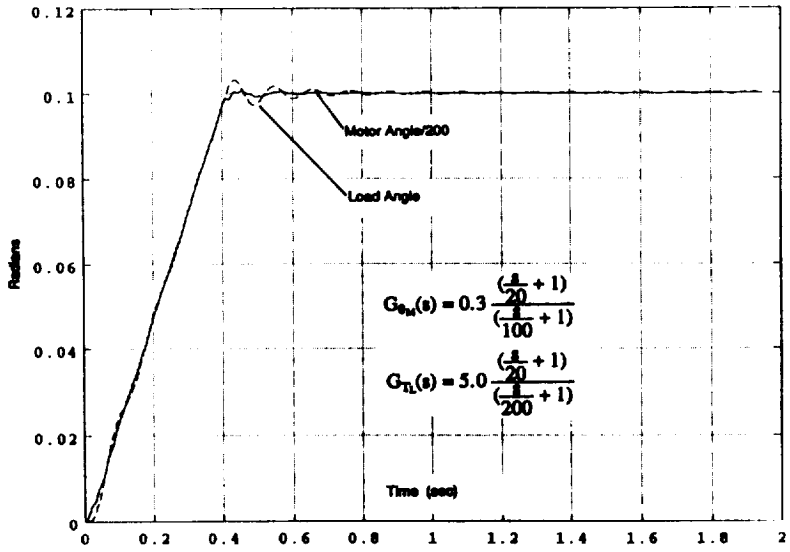

Figure 5: Position Slew With Colocated Position Control With Inner Torque Loop

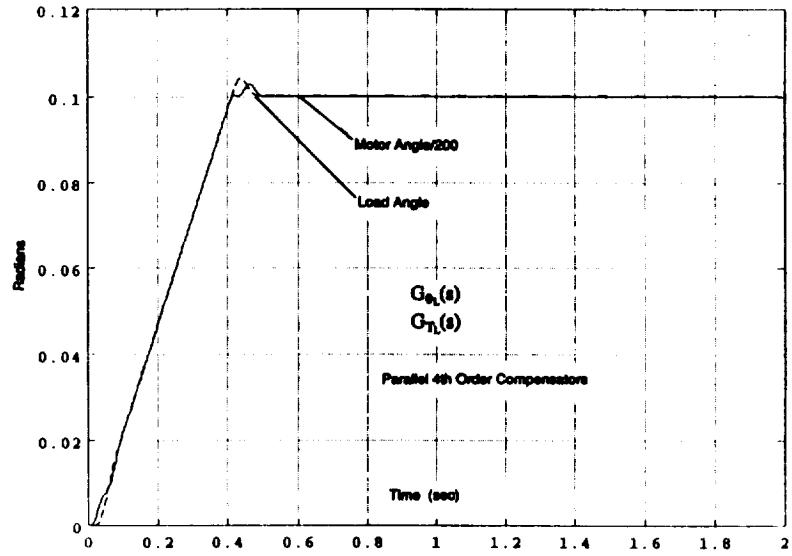

Figure 6: Position Slew With MIMO Controller

5. Summary

To summarize these results, a comparision is made of the position controllers with and without torque feedback and is shown in Figure 7. Torque feedback usage yields superior results over either colocated or noncolocated feedback used alone. Slew tracking errors are diminished and damping is improved thus reducing settling times. The qualitative results from this research are valid, although quantitative measures are difficult to extract as the controllers are not "normalized" to each other in terms of DC gain.

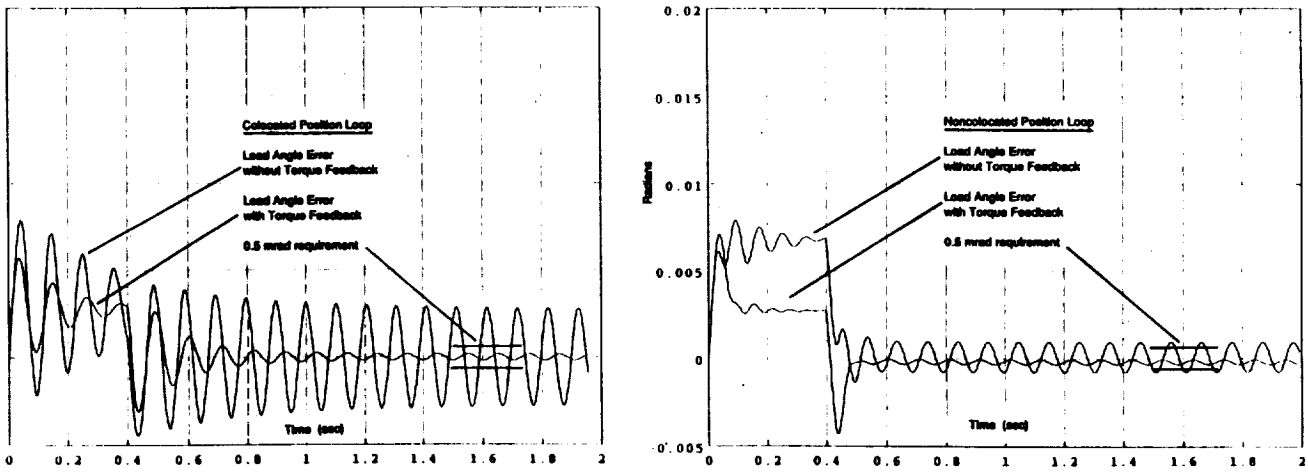

Figure 7: Servo Performance With and Without Inner Torque Loop

The nonlinear actuator model and control algorithms will be validated through hardware test as soon as the joint testbed is complete. Further analysis is also needed to create designs that provide robust torque control when the joint in contact (load is stationary). Parameter sensitivity studies and nonlinear limit cycle analysis using describing functions are planned to further investigate the spring stiffening and friction effects.

6. References

[1] Gretz, B. and Tilley, S., "Kinematics, Controls, and Path Planning Simulation Results for a Redundant Manipulator". In proceedings of NASA Conference on Space Telerobotics, Pasadena, California, January , 1989.

[2] Chun, W. and Brunson, P., "Actuators For A Space Manipulator". In proceedings of the Conference on Space Applications of AI and Robotics, NASA Goddard, May 13-14, 1987.

[3] Holzbock, W.G., Robotic Technology Principles and Practice. Published by Van Nostrand Reinhold Company, New York, New York, 1986.

[4] Wu, C. H. and Paul, R. P., "Manipulator Compliance Based on Joint Torque Control". In proceedings of the 19th IEEE Conference on Decision and Control, Vol. 1, pp. 84-88, Albuquerque, New Mexico, December, 1980.

[5] Pfeffer, L., Khatib, O., and Hake, J., "Joint Torque Sensory Feedback In The Control Of A PUMA Manipulator". In proceedings of the American Control Conference, pp. 818-824, Seattle, Washington, June, 1986.

[6] Hollars, M. G., Experiments in End-Point Control of Manipulators with Elastic Drives. PhD Thesis, Department of Aeronautics and Astronautics, Stanford University, May, 1988.

[7] Franklin, G.F., Powell, J.D. and A. Emami-Naeini, Feedback Control of Dynamic Systems. Published by Addison-Wesley Company, Reading, Massachusetts, 1986.

[8] Won, S.C., Lim, D.J. and D.H.Chyung, "DC Motor Driven Robotic Manipulator Control". In proceedings of 24th IEEE Conference on Decision and Control, Ft. Lauderdale, Florida, December, 1985.